

Generalizable Hyperparameter Optimization for Federated Learning on Non-IID Cancer Images

Elisa Gonçalves Ribeiro¹ ^a, Rodrigo Moreira¹ ^b,
Larissa Ferreira Rodrigues Moreira¹ ^c, André Ricardo Backes² ^d

¹*Institute of Exact and Technological Sciences, Federal University of Viçosa - UFV, Rio Paranaíba-MG, Brazil*

²*Department of Computing, Federal University of São Carlos, São Carlos-SP, Brazil*
 {elisa.ribeiro, rodrigo, larissa.f.rodrigues}@ufv.br, arbackes@yahoo.com.br

Keywords: Federated Learning, Hyperparameter Optimization, Non-IID Data, Medical Imaging, Cancer

Abstract: Deep learning for cancer histopathology training conflicts with privacy constraints in clinical settings. Federated Learning (FL) mitigates this by keeping data local; however, its performance depends on hyperparameter choices under non-independent and identically distributed (non-IID) client datasets. This paper examined whether hyperparameters optimized on one cancer imaging dataset generalized across non-IID federated scenarios. We considered binary histopathology tasks for ovarian and colorectal cancers. We perform centralized Bayesian hyperparameter optimization and transfer dataset-specific optima to the non-IID FL setup. The main contribution of this study is the introduction of a simple cross-dataset aggregation heuristic by combining configurations by averaging the learning rates and considering the modal optimizers and batch sizes. This combined configuration achieves a competitive classification performance.

1 INTRODUCTION

Cancer remains a leading global health burden, with projections of approximately 28.4 million new cases by 2040, and 35 million by 2050, representing increases of approximately 47% and 77%, respectively. Colorectal and ovarian cancers are particularly relevant, with colorectal cancer accounting for more than 1.9 million new cases and 930,000 deaths worldwide annually. Ovarian cancer causes approximately 314,000 new cases and 207,000 deaths annually and is frequently diagnosed at advanced stages, leading to high mortality rates (Morgan et al., 2022; Roshandel et al., 2024; Bray et al., 2024).

Deep learning has arisen as an approach for automated cancer diagnosis based on medical images. In histopathology, Convolutional Neural Networks (CNNs) and other deep architectures, often initialized with ImageNet weights, can achieve expert-level performance in distinguishing cancerous from non-cancerous tissues (Rodrigues and Backes, 2025). However, the standard centralized training paradigm,

in which large image collections are pooled in a single repository, conflicts with privacy regulations and institutional data governance, and the fact that data are naturally distributed across hospitals and laboratories (Guan et al., 2024).

Federated Learning (FL) has emerged as an alternative that enables collaborative training without sharing raw data. Institutions keep data on-site and periodically send model updates to a coordinating server, which aggregates them into a global server (McMahan et al., 2017; Rodrigues et al., 2025). FL has been applied to several medical imaging tasks, including brain tumor segmentation, chest X-ray classification, and computational pathology, achieving a performance close to centralized training while preserving data locality (Guan et al., 2024; Rodrigues Moreira et al., 2024; Barbosa et al., 2025).

However, practical deployment in clinical environments remains challenging because institutional datasets are rarely independent and identically distributed (IID). They differ in size, class balance, acquisition protocols, and patient demographics, which leads to strong non-independent and identically distributed (non-IID) client partitions and can degrade convergence and generalization (Rodrigues et al., 2025). In addition, FL models are sensitive to hyperparameter tuning, and hyperparameters tuned for

^a  <https://orcid.org/0009-0001-0882-1685>

^b  <https://orcid.org/0000-0002-9328-8618>

^c  <https://orcid.org/0000-0001-8947-9182>

^d  <https://orcid.org/0000-0002-7486-4253>

one site or dataset may transfer poorly to others, particularly under non-IID conditions. Existing studies on hyperparameter optimization (HPO) for FL often focus on a single dataset or assume fixed, task-specific configurations (Kuo et al., 2023; Kundroo and Kim, 2024); thus, obtaining hyperparameter configurations that generalize across non-IID federated cancer-imaging scenarios remains an open question.

In this paper, we address this gap by studying whether hyperparameters optimized on one cancer imaging dataset can be generalized across non-IID federated scenarios and across tumor types. We designed a two-phase pipeline that (i) performs centralized Bayesian HPO with the Tree-structured Parzen Estimator (TPE) on two binary histopathology tasks (ovarian and colon cancer) and (ii) transfers and combines the resulting configurations in a non-IID FL setup based on Federated Averaging (FedAvg). By comparing multiple CNN architectures under ovary-optimized, colon-optimized, and combined hyperparameter schemes, we assessed how these choices affect federated performance and whether simple combined configurations can act as robust strategies that generalize across non-IID federated cancer scenarios.

2 RELATED WORK

In this section we review prior work at the intersection of cancer imaging, HPO and federated or privacy preserving learning. Subramanian et al. (2022) addresses privacy-preserving classification of collaborative cancer models across heterogeneous, non-IID datasets. The authors propose a decentralized FL framework using FedAvg and FedProx, coupled with client-server Bayesian HPO and a selective update rule based on local performance improvement. Evaluating MobileNetV3, XceptionV3, and ResNet201 on CT and MRI data of cervical, lung, and colon cancers, they report accuracy, precision, recall, and F1 scores across varying communication rounds.

Khan et al. (2024) addresses automated breast cancer detection under privacy constraints and data scarcity. They proposed a decentralized federated framework where hospitals train CNNs using an ant colony optimization-based bilevel strategy for joint hyperparameter and architecture search, exchanging updates via a circular topology. Using the DDSM dataset distributed across three clients for binary classification, they show that the ant colony scheme outperforms particle swarm optimization (PSO) and grid search baselines in terms of accuracy.

Tamanini et al. (2025) focuses on efficient endometrioid ovarian carcinoma detection in

histopathology images with limited data. The pipeline extracts radiomics features from hematoxylin and eosin images converted into eight color spaces, applying incremental recursive feature elimination before training traditional classifiers and CNN baselines. The study reports that the YCrCb color space with Random Forest achieves nearly 98% accuracy.

Yang et al. (2025) addresses data-scarce skin cancer detection in IoT healthcare settings. The authors propose an active learning framework combining a CNN classifier with a reinforcement learning sample selector and an enhanced artificial bee colony algorithm for HPO. Evaluated on ISIC, HAM10000, and PH2 datasets, the approach shows consistent gains in accuracy and memory usage compared to various machine learning and deep learning baselines.

Li et al. (2025) optimizes hyperparameters for breast cancer classification to overcome the instability of existing metaheuristics. The authors introduce the Multi-Strategy Parrot Optimizer (MSPO), enhanced with Sobol initialization and chaotic perturbations, to tune a ResNet18 model. Benchmarked against CEC 2022 functions and applied to the BreakHis dataset, the MSPO-tuned model outperforms untuned versions and alternative algorithms in accuracy, precision, recall, and F1 score.

Almelibari (2025) tackles diabetes prediction while addressing privacy, class imbalance, and communication costs. The framework combines a tree-based and neural ensemble with a PSO-based weighting scheme, extended into a privacy-preserving federated architecture. Using SMOTE for class balancing on a public dataset, the study reports that their proposed weighted aggregation yields higher accuracy and communication efficiency.

We summarize our contribution in Table 1, where we use \bullet when the approach addresses the feature and \circ otherwise.

Contribution Positioning. While all solutions in Table 1 focus on improving cancer prediction or clinical decision support either by designing new FL protocols, proposing metaheuristic hyperparameter optimizers, or building more accurate centralized imaging pipelines, none of them investigates whether hyperparameters tuned on one dataset can generalize across non-IID federated cancer imaging scenarios and across tumor types. In this paper, we propose a two stage methodology that first performs Bayesian hyperparameter optimization on centralized histopathology tasks for colon and ovarian cancer and then transfers and combines the resulting configurations in a FL setup, enabling a controlled comparison across different CNNs and providing empirical

Table 1: Short comparison of the Related Works.

Approach	Cancer Task	Medical Imaging	Histopathology Images	Federated Learning	Non-IID Clients	HPO Focus	HPO in FL	Multiple Cancer Types
Subramanian et al. (2022)	●	●	○	●	●	●	●	●
Khan et al. (2024)	●	●	○	●	○	●	●	○
Tamanini et al. (2025)	●	●	●	○	○	○	○	○
Yang et al. (2025)	●	●	○	○	○	●	○	○
Li et al. (2025)	●	●	●	○	○	●	○	○
Almelibari (2025)	○	●	○	●	○	●	●	○
Our Approach	●	●	●	●	●	●	●	●

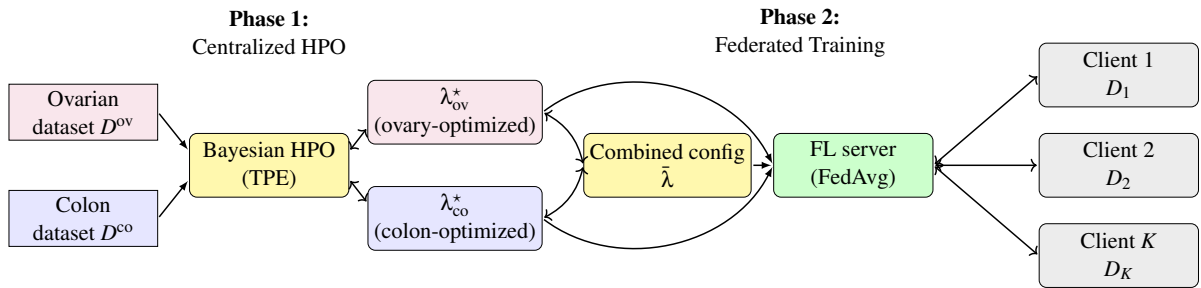


Figure 1: Proposed Method. Phase 1 performs centralized Bayesian hyperparameter optimization with TPE on ovarian and colon datasets, yielding task-specific optima λ_{ov}^* and λ_{co}^* and a combined configuration $\bar{\lambda}$. Phase 2 evaluates these three configurations in a non-IID federated setting using FedAvg.

evidence and practical guidelines on hyperparameter schemes that behave robustly under heterogeneous federated conditions.

3 MATERIAL AND METHODS

Figure 1 summarizes the proposed method. In Phase 1, we perform centralized Bayesian HPO with TPE on two binary histopathology tasks (ovarian and colon), obtaining dataset specific optima λ_{ov}^* and λ_{co}^* and constructing a combined configuration $\bar{\lambda}$ from them. In Phase 2, we instantiate a non-IID FL scenario with K clients trained with FedAvg, and evaluate these three hyperparameter schemes under identical model architectures and data partitions.

3.1 Medical Imaging Datasets

We consider two binary histopathology classification tasks, both framed as ‘‘cancer’’ vs. ‘‘non cancer’’. The first dataset is the Ovarian Cancer & Subtypes Histopathology dataset¹, which contains digital pathology patches extracted from hematoxylin and eosin (H&E) stained ovarian tissue slides. We group

the available subtypes into a single positive class (ovarian cancer) and use benign or non tumoral tissue as the negative class.

The second dataset is a subset of the LC25000 dataset², which contains colon histopathology images with normal and tumoral samples. We select only colon images and map them to a binary label (cancer vs. non cancer). Representative examples of ovarian and colon patches for both classes (Figure 2).

To enable a controlled comparison, we sub sample the LC25000 colon subset so that the resulting colon dataset matches the ovarian dataset in terms of total number of images and class imbalance ratio. After this alignment, the combined dataset comprises 996 images (ovary + colon). For each dataset, we randomly split the images into 80% for training and 20% for testing, with a stratified split on the binary label. Within the training portion, we further reserve a validation subset that is used exclusively for HPO. All images are resized to 224×224 pixels and normalized with ImageNet statistics.

3.2 CNN Architectures

We evaluate six CNNs that span from classic, low-depth models to more modern, parameter-efficient

¹<https://www.kaggle.com/datasets/bitsnpieces/ovarian-cancer-and-subtypes-dataset-histopathology>

²<https://www.kaggle.com/andrewmvd/lung-and-colon-cancer-histopathological-images>

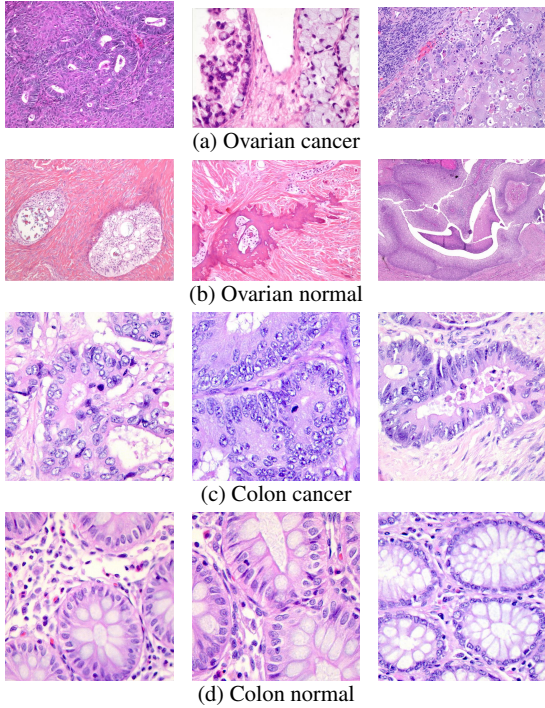


Figure 2: Examples of images from the two datasets used in this study.

networks. All models are initialized with ImageNet pretrained weights and adapted to binary classification by replacing the final fully connected layer.

- **AlexNet:** a CNN with five convolutional layers and three fully connected layers, included as a classical baseline for comparison with more recent architectures (Krizhevsky et al., 2012).
- **ResNet-18 / ResNet-34 / ResNet-50:** residual networks with increasing depth that use skip connections to ease optimization. ResNet-18 and ResNet-34 represent moderately deep backbones, while ResNet-50 provides a higher-capacity model built from bottleneck blocks (He et al., 2016).
- **SqueezeNet:** a compact architecture based on “fire” modules that reduces the number of parameters. It is included to assess whether lightweight models can achieve competitive performance in the federated histopathology setting (Rodrigues et al., 2025).
- **EfficientNet-B0:** a modern CNN obtained by compound scaling of depth, width, and resolution. It provides a strong parameter-efficient baseline and is particularly suited to capturing fine-grained texture patterns in histopathology images (Tan and Le, 2019).

3.3 Federated Learning Pipeline

We adopt a two phase pipeline that combines centralized HPO and federated training. In the first phase, we perform centralized training and evaluation on each dataset separately. Let D^{ov} denote the ovarian dataset and D^{co} the colon dataset. For each dataset, we fine tune ImageNet pretrained Convolutional Neural Network (CNN)s with a task specific classification head and use the validation split to drive HPO, as detailed in Section 3.4.

In the second phase, we simulate a cross silo federated learning scenario with K logical clients. The training data from D^{ov} and D^{co} are partitioned into K local datasets $\{D_k\}_{k=1}^K$ under a non-IID scheme that reflects realistic heterogeneity in clinical environments. Each client k receives a subset D_k characterized by different sample sizes and label proportions, so that the empirical label distribution $p_k(y)$ varies across clients. Federated training proceeds in communication rounds indexed by $t = 1, \dots, T$. At round t , the server broadcasts the current global parameters $\theta^{(t)}$ to all (or a subset of) clients, each client performs local stochastic gradient descent (SGD) updates for a fixed number of epochs on its local data, and the resulting local parameters $\{\theta_k^{(t+1)}\}_{k=1}^K$ are aggregated on the server using FedAvg (McMahan et al., 2017) (Equation: 1).

$$\theta^{(t+1)} = \sum_{k=1}^K \frac{n_k}{\sum_{j=1}^K n_j} \theta_k^{(t+1)}, \quad (1)$$

where $n_k = |D_k|$ is the number of training samples at client k . All federated experiments use the same CNN architectures and differ only in the hyperparameter configuration chosen for learning rate, optimizer, and batch size.

3.4 Hyperparameter Optimization

For each dataset $D \in \{D^{\text{ov}}, D^{\text{co}}\}$ we perform centralized HPO using the Tree structured Parzen Estimator (TPE) algorithm (Bergstra et al., 2011). Let λ denote a hyperparameter configuration (Equation 2),

$$\lambda = (\eta, o, b), \quad (2)$$

where $\eta \in \Lambda_\eta$ is the learning rate, $o \in \Lambda_o$ is the optimizer (e.g., SGD, Adam), and $b \in \Lambda_b$ is the batch size. Given a configuration λ , we train the model on the training split of D and evaluate the resulting parameters on the validation split, obtaining a scalar performance metric $f(\lambda; D)$. The goal is to solve the Equation 3:

$$\lambda^*(D) = \arg \max_{\lambda \in \Lambda} f(\lambda; D), \quad (3)$$

where $\Lambda = \Lambda_\eta \times \Lambda_o \times \Lambda_b$ is the search space.

The TPE algorithm models the conditional density $p(\lambda | f)$ as a mixture of two densities over “good” and “bad” configurations and selects new candidates that maximize the expected improvement (Bergstra et al., 2011; Rodrigues et al., 2020). After a fixed budget of evaluations, we obtain two dataset specific optima defined in Equation 4:

$$\lambda_{\text{ov}}^* = \lambda^*(D^{\text{ov}}), \quad \lambda_{\text{co}}^* = \lambda^*(D^{\text{co}}). \quad (4)$$

Table 2: Hyperparameter Search Space.

Hyperparameter	Distribution	Search Space
Learning Rate (LR)	Log-Uniform	$1 \times 10^{-5}, 1 \times 10^{-3}$
Batch Size	Categorical	{16, 32, 64}
Optimizer	Categorical	{Adam, SGD}

These configurations are later transferred to the federated phase and used as baselines. The search space for HPO was defined and explored by TPE, as detailed in Table 2. The hyperparameters tuned in this study were as follows:

- **Learning rate:** regulates the magnitude of each update applied to the model parameters during gradient-based optimization. We defined its search space on a logarithmic scale, which is a common choice for quantities that span several orders of magnitude, enabling the optimizer to probe the model’s sensitivity to different LR values more effectively (Goodfellow et al., 2016; Rodrigues et al., 2020).
- **Batch size:** specifies how many training samples are used to compute each gradient update. It was treated as a discrete variable selected from a set of candidate values as it affects both the convergence behavior and computational efficiency (Goodfellow et al., 2016; Rodrigues et al., 2020).
- **Optimizer:** the optimization algorithm that updates the network weights to reduce the loss function. We modeled the optimizer choice as a categorical hyperparameter and allowed TPE to select the most suitable option for each configuration (Goodfellow et al., 2016).

3.5 Combined Hyperparameter Aggregation Heuristic

The main contribution of this study is a simple yet explicit aggregation heuristic that combines dataset-specific optima into a single combined hyperparameter configuration. We aim to turn the optima obtained for distinct cancer tasks into a transparent candidate for generalizable hyperparameters in non-IID FL.

Let the optimal configurations found by TPE on the ovarian and colon datasets be given according to Equation 5:

$$\lambda_{\text{ov}}^* = (\eta_{\text{ov}}, o_{\text{ov}}, b_{\text{ov}}), \quad \lambda_{\text{co}}^* = (\eta_{\text{co}}, o_{\text{co}}, b_{\text{co}}), \quad (5)$$

where η is the learning rate, o is the optimizer, and b is the batch size. Based on the two optima, we define the combined configuration $\bar{\lambda}$ as shown in Equation 6.

$$\bar{\lambda} = (\bar{\eta}, \bar{o}, \bar{b}), \quad (6)$$

With the learning rate given by the arithmetic mean, as defined in Equation 7:

$$\bar{\eta} = \frac{\eta_{\text{ov}} + \eta_{\text{co}}}{2}, \quad (7)$$

and the optimizer and batch size obtained as modal choices among the dataset specific optima:

$$\bar{o} = \text{mode}\{o_{\text{ov}}, o_{\text{co}}\}, \quad \bar{b} = \text{mode}\{b_{\text{ov}}, b_{\text{co}}\}. \quad (8)$$

In case of a tie in Equation (8) (for example, different optimizers selected for each dataset with equal frequency), we break ties by choosing the value associated with the higher validation F1 score in the centralized phase. Algorithm 1 summarizes the construction of $\bar{\lambda}$.

Algorithm 1 Combined hyperparameter configuration from dataset specific optima

Require: Optimal configurations $\lambda_{\text{ov}}^* = (\eta_{\text{ov}}, o_{\text{ov}}, b_{\text{ov}})$ and $\lambda_{\text{co}}^* = (\eta_{\text{co}}, o_{\text{co}}, b_{\text{co}})$, validation scores $f(\lambda_{\text{ov}}^*; D^{\text{ov}})$ and $f(\lambda_{\text{co}}^*; D^{\text{co}})$

- 1: Compute averaged learning rate according to Equation (7):

$$\bar{\eta} \leftarrow \frac{\eta_{\text{ov}} + \eta_{\text{co}}}{2}.$$

- 2: Set candidate sets for optimizer and batch size:

$$O \leftarrow \{o_{\text{ov}}, o_{\text{co}}\}, \quad \mathcal{B} \leftarrow \{b_{\text{ov}}, b_{\text{co}}\}.$$

- 3: Compute $\bar{o} \leftarrow \text{mode}(O)$; if there is a tie, choose the optimizer associated with the higher validation F1 score.

- 4: Compute $\bar{b} \leftarrow \text{mode}(\mathcal{B})$; if there is a tie, choose the batch size associated with the higher validation F1 score.

- 5: **return** $\bar{\lambda} = (\bar{\eta}, \bar{o}, \bar{b})$ as in Equation (6).

In the federated setting, we therefore evaluate three hyperparameter schemes: (i) λ_{ov}^* (ovary optimized), (ii) λ_{co}^* (colon optimized), and (iii) $\bar{\lambda}$ (combined), defined in Equations (5) and (6). All other

components of the pipeline were fixed. This design isolates the impact of hyperparameter selection on federated performance and frames the combined configuration as a strategy across diverse datasets in non-IID federated cancer imaging scenarios.

4 RESULTS AND DISCUSSION

We carried out all experiments on a Dell Precision 5860 workstation equipped with an Intel Xeon w3-2435 processor (8 CPU cores at 3.1 GHz), 64 GB of DDR5 memory, and an NVIDIA RTX 4000 Ada Generation GPU with 20 GB of VRAM. We implemented the training, validation, and testing using the Flower (Beutel et al., 2020) framework, and adopted FedAvg (McMahan et al., 2017) as the aggregation algorithm.

HPO for each CNN is performed centrally with TPE, using the Hyperopt (Bergstra et al., 2015) library. We construct the combined configuration $\bar{\lambda}$ via the proposed aggregation heuristic. In the federated experiments, we keep the model architectures, data partitions, and number of local epochs and communication rounds fixed, and vary only the hyperparameter scheme (colon-optimized, ovary-optimized, or combined).

4.1 Centralized HPO

We first investigate the behavior of each CNN under centralized training, using TPE to obtain dataset specific hyperparameter optima. This experiment provides two baselines: it characterizes how well each architecture fits the colon and ovarian tasks in isolation, and it yields the colon optimized and ovary optimized configurations that will later be transferred to the federated setting and combined through the heuristic. Table 3 summarizes the best batch size, optimizer, and validation loss found by TPE for each CNN and dataset, while the corresponding learning rates are reported in Table 4.

On the colon task, all models converged with Adam and batch sizes between 16 and 64, with small learning rates across architectures. The lowest validation loss was obtained by ResNet18 (best loss 2.49×10^{-5} with batch size 32), followed by ResNet50 and SqueezeNet, which indicates that shallow residual networks and lightweight architectures can fit the colon dataset under centralized training.

On the ovarian task, TPE again selected small learning rates and batch sizes between 16 and 64, but the ranking of architectures changed. EfficientNet-B0 achieved the lowest validation loss (1.02×10^{-1} with

Table 3: Best batch size, optimizer, and validation loss found by TPE.

Dataset	Model	Batch size	Optimizer	Best val. loss
Colon	AlexNet	16	Adam	3.71×10^{-4}
	ResNet-50	32	Adam	1.39×10^{-4}
	ResNet-34	64	Adam	1.86×10^{-4}
	ResNet-18	32	Adam	2.49×10^{-5}
	SqueezeNet 1.1	16	Adam	1.57×10^{-4}
	EfficientNet-B0	32	Adam	4.59×10^{-4}
Ovary	AlexNet	64	Adam	2.00×10^{-1}
	ResNet-50	64	Adam	1.84×10^{-1}
	ResNet-34	64	Adam	1.83×10^{-1}
	ResNet-18	32	Adam	2.16×10^{-1}
	SqueezeNet 1.1	16	SGD	2.96×10^{-1}
	EfficientNet-B0	64	Adam	1.02×10^{-1}

Table 4: Best Learning rates found by TPE.

Model	η_{co}	η_{ov}	$\bar{\eta}$
AlexNet	1.28×10^{-4}	9.06×10^{-5}	1.09×10^{-4}
ResNet-50	2.22×10^{-4}	2.49×10^{-5}	1.23×10^{-4}
ResNet-34	1.59×10^{-4}	3.86×10^{-5}	9.88×10^{-5}
ResNet-18	2.90×10^{-4}	3.12×10^{-5}	1.61×10^{-4}
SqueezeNet 1.1	8.38×10^{-5}	3.78×10^{-4}	2.31×10^{-4}
EfficientNet-B0	5.99×10^{-4}	9.64×10^{-4}	7.82×10^{-4}

batch size 64), while ResNet50 and ResNet34 exhibited similar losses around 1.8×10^{-1} . This shift suggests that architectures with more expressive feature extractors, such as EfficientNet-B0, are better suited to capture the higher intra-class variability of ovarian histopathology compared to the colon dataset. These dataset-specific optima, λ_{ov}^* and λ_{co}^* , provide the starting point for the federated experiments and for the combined configuration.

4.2 Federated Performance Under Different Hyperparameter Schemes

In the federated setting we analyze how the three hyperparameter schemes affect performance on the joint non-IID ovarian+colon scenario. Table 5 reports the federated results on the combined non-IID ovarian+colon scenario for each CNN and for the three hyperparameter schemes (see Section 3.5).

All experiments use 50 local epochs and 3 communication rounds, so differences in performance can be attributed to the choice of learning rate, optimizer, and batch size. For each CNN, the best result across the three schemes is underlined in the table to highlight the most effective configuration.

For ResNet50, the ovary-optimized configuration yields the best federated performance, with accuracy 0.955 and F1-score 0.953, slightly outperforming the

Table 5: Federated performance on the non-IID scenario under three hyperparameter schemes.

Model	Colon-optimized				Ovary-optimized				Combined			
	Acc	Prec	Rec	F1	Acc	Prec	Rec	F1	Acc	Prec	Rec	F1
AlexNet	0.905	0.906	0.905	0.896	0.890	0.885	0.890	0.882	<u>0.905</u>	<u>0.906</u>	<u>0.905</u>	<u>0.896</u>
ResNet-18	0.890	0.897	0.890	0.875	0.870	0.868	0.870	0.852	<u>0.920</u>	<u>0.921</u>	<u>0.920</u>	<u>0.914</u>
ResNet-34	0.910	0.919	0.910	0.899	0.920	0.921	0.920	0.914	<u>0.920</u>	<u>0.923</u>	<u>0.920</u>	<u>0.913</u>
ResNet-50	0.950	0.949	0.950	0.949	<u>0.955</u>	<u>0.957</u>	<u>0.955</u>	<u>0.953</u>	0.935	0.940	0.935	0.930
SqueezeNet	0.915	0.916	0.915	0.908	<u>0.955</u>	<u>0.954</u>	<u>0.955</u>	<u>0.954</u>	0.915	0.914	0.915	0.910
EfficientNet-B0	0.890	0.903	0.890	0.873	0.865	0.884	0.865	0.836	<u>0.900</u>	<u>0.906</u>	<u>0.900</u>	<u>0.888</u>

colon-optimized (F1 0.949) and combined (F1 0.930) settings. ResNet34 follows a similar pattern: F1-score of 0.914 for the ovary-optimized configuration, compared to 0.899 (colon-optimized) and 0.913 (combined).

In contrast, ResNet18 and EfficientNet-B0 benefit more from the combined configuration. ResNet18 achieves the highest F1-score (0.914) and accuracy (0.920), clearly improving over the colon-optimized (F1 = 0.875) and ovary-optimized (F1 = 0.852) settings. For EfficientNet-B0, the combined configuration attains an F1-score of 0.888, outperforming both colon-optimized (0.873) and ovary-optimized (0.836) schemes. These trends are summarized in Figure 3.

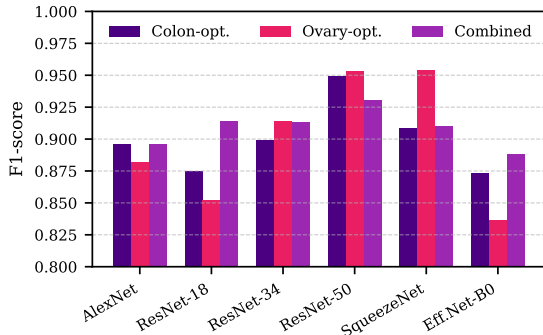


Figure 3: Federated F1-score for each non-IID scenario evaluated.

AlexNet and SqueezeNet illustrate that no single dataset-specific optimum is universally dominant. AlexNet reaches its best F1-score under the colon-optimized configuration (F1 = 0.896), with the combined scheme matching this value and the ovary-optimized configuration slightly worse. For SqueezeNet, the ovary-optimized configuration with SGD achieves the highest F1-score (0.954), while the colon-optimized and combined schemes remain competitive around 0.908–0.910. When averaging across all CNNs, the combined configuration achieves the highest mean F1-score (0.909), compared to 0.900

for the colon-optimized and 0.899 for the ovary-optimized schemes.

5 CONCLUSION

This study investigated whether hyperparameters optimized on one cancer histopathology dataset can generalize across non-IID federated scenarios and tumor types. Centralized experiments showed that CNNs respond differently to the colon and ovarian tasks, with lightweight and moderately deep models (such as ResNet18) fitting the colon dataset particularly well, whereas EfficientNet-B0 achieved the best validation loss on ovarian images. In the federated non-IID setting, the ovary-optimized configuration tended to favor deeper residual networks (e.g., ResNet50), whereas the combined configuration proved beneficial for lighter models, such as ResNet18 and EfficientNet-B0. When averaged across all architectures, the combined scheme achieved the highest mean F1-score and the lowest mean validation loss among the three hyperparameter schemes, indicating that the proposed aggregation heuristic can serve as a choice in a challenging non-IID scenario.

ACKNOWLEDGMENTS

The authors gratefully acknowledge the financial support of FAPEMIG (Grant #APQ00923-24) and the Institutional Program for Scientific Initiation Scholarships (PIBIC) at the Federal University of Viçosa (UFV). André R. Backes gratefully acknowledges the financial support of CNPq (Grant #302790/2024-1).

REFERENCES

Almelibari, A. A. (2025). Enhancing diabetes disease prediction and privacy preservation via federated learning

and pso-wco optimization. *Statistics, Optimization & Information Computing*, 14:2297–2311.

Barbosa, G. V. G., Ferreira Rodrigues, L. G., F. Rodrigues Moreira, L., and Backes, A. R. (2025). Federated Learning in Breast Cancer Diagnosis. *Revista de Informática Teórica e Aplicada*, 32(1):173–179.

Bergstra, J., Bardenet, R., Bengio, Y., and Kégl, B. (2011). Algorithms for Hyper-Parameter Optimization. In *Advances in Neural Information Processing Systems*, volume 24. Curran Associates, Inc.

Bergstra, J., Komer, B., Eliasmith, C., Yamins, D., and Cox, D. D. (2015). Hyperopt: a Python library for model selection and hyperparameter optimization. *Computational Science & Discovery*, 8(1):014008.

Beutel, D. J., Topal, T., Mathur, A., Qiu, X., Fernandez-Marques, J., Gao, Y., Sani, L., Li, K. H., Parcollet, T., De Gusmão, P. P. B., et al. (2020). Flower: A friendly federated learning research framework. *arXiv preprint arXiv:2007.14390*.

Bray, F., Laversanne, M., Sung, H., Ferlay, J., Siegel, R. L., Soerjomataram, I., and Jemal, A. (2024). Global cancer statistics 2022: GLOBOCAN estimates of incidence and mortality worldwide for 36 cancers in 185 countries. *CA: A Cancer Journal for Clinicians*, 74(3):229–263.

Goodfellow, I., Bengio, Y., and Courville, A. (2016). *Deep Learning*. MIT Press. <http://www.deeplearningbook.org>.

Guan, H., Yap, P.-T., Bozoki, A., and Liu, M. (2024). Federated learning for medical image analysis: A survey. *Pattern Recognition*, 151:110424.

He, K., Zhang, X., Ren, S., and Sun, J. (2016). Deep Residual Learning for Image Recognition. In *2016 IEEE Conference on Computer Vision and Pattern Recognition (CVPR)*, pages 770–778.

Khan, S., Nosheen, F., Naqvi, S. S. A., Jamil, H., Faseeh, M., Ali Khan, M., and Kim, D.-H. (2024). Bilevel hyperparameter optimization and neural architecture search for enhanced breast cancer detection in smart hospitals interconnected with decentralized federated learning environment. *IEEE Access*, 12:63618–63628.

Krizhevsky, A., Sutskever, I., and Hinton, G. E. (2012). ImageNet Classification with Deep Convolutional Neural Networks. In *Advances in Neural Information Processing Systems 25*, pages 1097–1105. Curran Associates, Inc.

Kundroo, M. and Kim, T. (2024). Demystifying impact of key hyper-parameters in federated learning: A case study on cifar-10 and fashionmnist. *IEEE Access*, 12:120570–120583.

Kuo, K., Thaker, P., Khodak, M., Nguyen, J., Jiang, D., Talwalkar, A., and Smith, V. (2023). On Noisy Evaluation in Federated Hyperparameter Tuning. In *Proceedings of Machine Learning and Systems*, volume 5, pages 127–144. Curan.

Li, H., Govindarajan, V., Ang, T. F., Shaikh, Z. A., Ksibi, A., Chen, Y.-L., Ku, C. S., Leong, M. C., Shabaruddin, F. H., Ishak, W. Z. W., and Por, L. Y. (2025). Mspo: A machine learning hyperparameter optimization method for enhanced breast cancer image classification. *DIGITAL HEALTH*, 11:20552076251361603.

McMahan, B., Moore, E., Ramage, D., Hampson, S., and Arcas, B. A. y. (2017). Communication-Efficient Learning of Deep Networks from Decentralized Data. In Singh, A. and Zhu, J., editors, *Proceedings of the 20th International Conference on Artificial Intelligence and Statistics*, volume 54, pages 1273–1282. PMLR.

Morgan, E., Arnold, M., Gini, A., Lorenzoni, V., Cabasag, C. J., Laversanne, M., Vignat, J., Ferlay, J., Murphy, N., and Bray, F. (2022). Global burden of colorectal cancer in 2020 and 2040: incidence and mortality estimates from GLOBOCAN. *Gut*, 72(2):338–344.

Rodrigues, L. F., Naldi, M. C., and Mari, J. F. (2020). Comparing convolutional neural networks and preprocessing techniques for HEp-2 cell classification in immunofluorescence images. *Computers in Biology and Medicine*, 116:103542.

Rodrigues, Moreira, L. F. and Backes, A. R. (2025). Ensemble of handcrafted and learned features for colorectal cancer classification. *Journal of Imaging Informatics in Medicine*.

Rodrigues, L. G. F., V. Gomes Barbosa, G., Moreira, R., Rodrigues Moreira, L. F., and Backes, A. R. (2025). Medical image classification with privacy: Centralized and federated learning comparison. *Revista de Informática Teórica e Aplicada*, 32(1):180–187.

Rodrigues Moreira, L. F., Moreira, R., Martins, E. T., Jansen, V. F., Lima, Y. S., Rodrigues, L. G. F., Travençolo, B. A. N., and Backes, A. R. (2024). Maximizing the Power of Cognitive Services with an AI-as-a-Service Architecture for Seamless Delivery. In *2024 IEEE 13th International Conference on Cloud Networking (CloudNet)*, pages 1–8, Rio de Janeiro, Brazil. IEEE.

Roshandel, G., Ghasemi-Kebria, F., and Malekzadeh, R. (2024). Colorectal Cancer: Epidemiology, Risk Factors, and Prevention. *Cancers*, 16(8).

Subramanian, M., Rajasekar, V., V. E., S., Shanmugavadi, K., and Nandhini, P. S. (2022). Effectiveness of Decentralized Federated Learning Algorithms in Healthcare: A Case Study on Cancer Classification. *Electronics*, 11(24).

Tamanini, B., Sousa, V., Rodrigues, L., Oliveira, D., Dias, C., Cruz, L., Diniz, J., and Júnior, L. S. (2025). Classificação de Carcinoma Endometriode de Ovário por Transformação de Esquema de Cor e Radiomics em Imagens Histopatológicas. In *Anais do XXV Simpósio Brasileiro de Computação Aplicada à Saúde*, pages 68–79, Porto Alegre, RS, Brasil.

Tan, M. and Le, Q. V. (2019). Efficientnet: Rethinking model scaling for convolutional neural networks. *CoRR*, abs/1905.11946.

Yang, J., Qin, H., Wang, J., Yee, P. L., Prajapat, S., Kumar, G., Balusamy, B., Bashir, A. K., and Omar, M. (2025). IoT-Driven Skin Cancer Detection: Active Learning and Hyperparameter Optimization for Enhanced Accuracy. *IEEE Journal of Biomedical and Health Informatics*, pages 1–11.